Graphene-doped photo-patternable ionogels: tuning of conductivity and mechanical stability of 3D microstructures.

Mohamed Oubaha[a*], Andrew Kavanagh[b], Arnaud Gorin[a], Gabija Bickauskaite[c], Robert Byrne[b], Maria Farsari[c], Richard Winfield[d], Dermot Diamond[b], Colette McDonagh[a] and Robert Copperwhite[a]

a: Optical Sensors Laboratory, National Centre for Sensor Research, Dublin City University, Glasnevin, Dublin 9, Ireland.

b: CLARITY: The Centre for Sensor Web Technologies, National Centre for Sensor Research, Dublin City University, Glasnevin, Dublin 9, Ireland.

c: Institute of Electronic Structure and Laser, Foundation for Research and Technology Hellas, N. Plastira 100, GR-70013 Heraklion, Crete, Greece.

d: Tyndall National Institute, Cork, Ireland

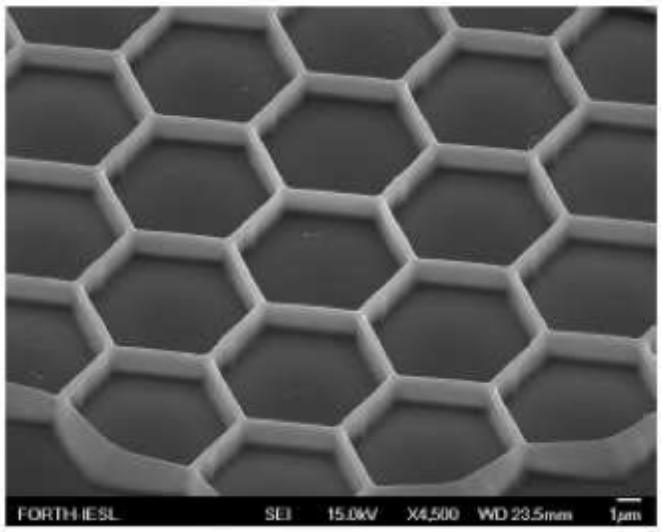

Graphene-like Structure Fabricated by Multi-Photon Polymerisation of Hybrid Ionogels.

Abstract

This work reports for the first time the development of enhanced conductivity, graphene-doped photo-patternable hybrid organic-inorganic ionogels and the effect of the subsequent materials condensation on the conductivity and mechanical stability of three-dimensional microstructures fabricated by multi-photon polymerisation (MPP). Ionogels were based on photocurable silicon/zirconium hybrid sol-gel materials and phosphonium (trihexyltetradecylphosphonium dicyanamide [P6,6,6,14][DCA] ionic liquid (IL). To optimise the dispersion of graphene within the ionogel matrices, aqueous solutions of graphene were prepared, as opposed to the conventional graphene powder approach, and employed as catalysts of hydrolysis and condensation reactions occurring in the sol-gel process.

Ionogels were prepared via a two step process by varying the hydrolysis degree from 25 to 50%, IL content between 0-50 w/w%, and the inorganic modifier (zirconate complex) concentration from 30 to 60 mol.% against the photocurable ormosil and they were characterised via Raman, Electrochemical Impedance Spectroscopy and Transmission Electron Microscopy. MPP was performed on the hybrid ionogels, resulting in three-dimensional microstructures that were characterised using scanning electron microscopy.

It is clearly demonstrated that the molecular formulation of the ionogels, including the concentration of graphene and the zirconate network modifier, play a critical role in the conductivity of the ionogels and influence the resulting mechanical stability of the fabricated three-dimensional microstructures. This work aims to establish for the first time the relationship between the molecular design and condensation of materials in the physico-chemistry and dynamic of ionogels.

Introduction

Ionogels are currently the subject of a rapidly growing number of both fundamental and applied studies in materials science. They are a new type of hybrid material which consist of an ionic liquid (IL) confined within the backbone of a gel-like structure [1, 2, 3]. ILs can be generally described as organic salts combining many favourable physicochemical properties including low melting points (typically <370 K), negligible vapour pressure, high ionic conductivities and thermal stability [4, 5]. This has made ILs interesting candidates for a number of applications including electrolytes for solar-cells [6], fluorescent [7] and optical devices [8].So far, two routes have been highlighted for the incorporation of ILs in a gel; the organic route, which involves in situ polymerization or swelling of polymers with ILs [9, 10], and the inorganic route, which consists of impregnation of ILs within oxide backbones [11]. Of the inorganic routes, the polymeric sol-gel process is probably the most popular synthetic route, as recently summarized in an excellent review [2]. It involves hydrolysis and condensation reactions of inorganic or hybrid precursors in order to develop inorganic backbones with morphologies ranging from macroporous materials to dense bulk materials depending on the hydrolysis conditions and the nature of the precursors employed. The sol–gel chemistry is therefore well known and is detailed in a number of reviews [12, 13, 14] and books [15, 16].

The incorporation of ILs within sol-gel materials has been reported mainly on silicate based materials, where confinement and dynamics of ILs within mesoporous structures has been demonstrated [17, 18, 19]. However, one major disadvantage of these materials is their limited mechanical resistance due to the low connectivity of the inorganic network, because of the low drying temperatures (to avoid degradation of the organic moieties in ILs), and the characteristic liquid property of the ILs. This often results in leaching and miniaturisation issues that are critical parameters for all- solid-state devices. Furthermore, to our knowledge, no study has so far investigated the effect of the condensation of the inorganic backbone on the IL dynamic and the subsequent conductivity.

An interesting approach to improve on the existing conductivity properties of solid- state electrolytes consists of the addition of co-encapsulants that exhibit electronic conductivity [20]. Arguably the most popular avenue of choice it to use materials derived from the carbon allotrope *graphite,* which is composed of multiple stacked sheets of aromatic sp2-hybridised atoms that exist in the third dimension [21]. Graphite single two-dimensional sheets (graphene) can be obtained by a chemical reduction process of graphite in aqueous solutions [22, 23, 24, 25] and rolled up to form one-dimensional nanotubes [26]. When combined with ionogels, so called *"bucky gels"* therefore unite the electron conducting properties of graphite-based materials with the ionic conducting ILs in the solid state [27].

Composites based on ILs and materials derived from graphite are easily prepared [28] by simply mixing and sonicating the two independent liquid phases [29], or by mixing and grinding graphene powder with an IL in an agar plate, to produce the gel-like material [30]. Another important aspect for the development of the next generation of solid-state electrolytes and electro-optical systems is the shaping and miniaturisation on substrates of diverse forms.

A possible solution to these major issues has recently been proposed by our group, which is to develop photocurable ionogels that can be photo-structured to submicron resolution as both planar and 3D patterns employing both single and multi-photon polymerisation (MPP) techniques [31]. The principle of confining ILs within photopatternable silicon/zirconium hybrid materials has been demonstrated and their conductivity and electrochromic behaviour correlated to the IL concentrations. In comparison to the relatively simple silicate-based sol-gel matrices employed so far in the development of ionogels, our materials contain an additional transition metal inorganic network, which further increases the connectivity of the inorganic network at ambient temperatures [32]. Furthermore, the occurrence of photopolymerisation reactions leads to the formation of an organic network overlapping both inorganic networks (silicate and zirconate). This additional double capability of polymerisation dramatically increases the condensation of the sol-gel matrices and contributes to a better confinement of the IL within the mesopores of the sol-gel

matrices, thereby minimizing IL leaching.

Herein we report, the first study on the effect of the condensation of hybrid sol-gel materials on the physical properties of ILs, and the impact of the IL concentration on the photoreactivity and mechanical stability of 3D photopatterned microstructures fabricated by MPP. In addition to this, a novel sol-gel synthesis, employing aqueous solutions of graphene, is proposed for the development of the materials. This original strategy is proposed in order to ensure the highest possible dispersion of graphene during the sol-gel synthesis and in the subsequent ionogel materials as well as to investigate its effect on the overall conductivity of the ionogels.

Experimental

Chemicals and materials

Trihexyltetradecylphosphonium dicyanamide [P6,6,6,14] [DCA] was obtained as a complimentary sample from Cytec® Industries. Further purification was achieved by washing with both water and hexane, and by column chromatography. ILs were then dried under vacuum at 40°C for 48 h, and stored under argon at 20°C [33]. Poly(3-octylthiophene-2,5-diyl) (POT), 3-methacryloxypropyltrimethoxysilane (MAPTMS, assay 99% in methanol), zirconium(IV) n-propoxide (ZPO, assay ~70% in propanol) and methacrylic acid (MAAH, C4H6O2, assay ~98%), were used as purchased from Sigma-Aldrich® Ireland. Diethylaminobenzophenone (DEABPH) was purchased from Alpha Aesar and used without any further purification.

Graphene solution preparation

Graphite powder was purchased from Sigma Aldrich and sieved through a 0.5 mm mesh to remove large particles. Sodium dodecylbenzene sulfonate (SDBS) was purchased from Sigma and used as provided. A 0.5 mg/ml solution of SDBS in deionised water was prepared. The graphene dispersion was prepared by adding 1 mg/ml of sieved graphite to the SDBS solution and sonicating in a low power sonic bath for 24 hrs. The dispersion was then centrifuged for 90 min at 2000 rpm. The concentration was calculated by filtering 10 ml of the

dispersion through a weighed filter paper, washing with 100 ml of dionised water, drying in a vacuum oven overnight and measuring the mass deposited.

Hybrid sol-gel synthesis

The sol–gel synthesis was based on the formation of stable and homogeneous solutions obtained from the reaction between photosensitive organically modified precursors MAPTMS, ZPO and MAAH which were allowed to react in different molar ratios leading to materials A to G, as shown in Table 1.

For the synthesis of material A, MAPTMS was pre-hydrolysed with an aqueous solution (HCl 0.005 N), employing a 1.00 : 0.75 water to alkoxide molar ratio. For the synthesis of materials B to G the pre-hydrolysis of the organosilane precursor was performed employing an aqueous solution containing 0.22 mg/ml of graphene. Before use, this solution was acidified with an aqueous solution of HCl (0.05 M) to obtain an aqueous solution of pH 2.3

After 20 min of stirring, the solution became fully transparent demonstrating the occurrence of hydrolysis and condensation reactions leading to the production of alcohol that allows the miscibility of all species present in solution. In parallel, to control the hydrolysis–condensation of ZPO and avoid the formation of any undesired ZrO2 precipitate, MAAH was used, in 1/1 stoichiometric ratio against ZPO, as a chelating agent as it covalently binds with the zirconium atom

through two oxygen atoms. After 45 minutes of reaction, the pre-hydrolysed MAPTMS solution was added drop-wise to the zirconium complex.

Following another 45 minutes of reaction, in order to improve the homogeneity of both molecular systems, a second hydrolysis employing water (pH 7) was performed leading to a hydrolysis of 50% mol. of the total alkoxide groups. To keep the quantity of graphene constant in materials C-G, adjustment of the amount of graphene was also performed by using the parent aqueous graphene solution during the second hydrolysis. The final sol was left stirring for 24 hours before use.

Sol-gel Formulation	*MAPTMS (mol%)*	*ZPO/MAAH (mol.%)*	*Graphene (mg/ml of sol-gel)*	*Hydrolysis Degree (mol. %)*
A	70	30	0	10
B	70	30	0.0078	25
C	70	30	0.0157	50
D	60	40	0.0157	50
E	55	45	0.0157	50
F	50	50	0.0157	50
G	40	60	0.0157	50

Table 1. Ionogel formulations

Ionogel synthesis

e.g. sol-gel A : [P6,6,6,14][DCA] 50 : 50 w/w.All ionogel formulations were photopolymerised using the *in situ* technique. For the cited example the preparation was as follows:500 mg of sol-gel solution was mixed thoroughly with 500 mg of [P6,6,6,14][DCA] and 10 mg of photoinitiator (DEABPH). The ionogel solution was then sonicated for 5 minutes to ensure the photoinitiator was dissolved fully. It was then transferred to a 2 cm diameter circular mould and photopolymerized with a UV BondWand (Electro- lite, Connecticut 20 W, 365 nm) for 10 minutes. The ionogel was placed in a vacuum oven at 50°C for 24 hours. All ionogel combinations were prepared in accordance with the above procedure, with adjustments only to the hybrid organic sol–gel composition.

3D Structuring of Ionogels

The experimental setup employed for the fabrication of three-dimensional microstructures has been described extensively previously [34, 35, 36]. A Ti:Sapphire femtosecond laser (Femtolasers Fusion, 800 nm, 75MHz, <20fs) beam was focused into the photopolymerisable composite using a high numerical aperture focusing microscope objective lens (100x, N.A. = 1.4, Zeiss, Plan Apochromat). Sample movement was achieved using piezoelectric and linear stages, for fine and step movement, respectively (PI). The direct laser writing setup

was computer-controlled using 3DPoli software. Woodpile structures of dimensions 20x20 μm x 10 μm height and of 1 μm period were fabricated. The average power used for the fabrication of the high-resolution structures was in the range 3 to 7 mW, measured before the objective, while the average transmission was 20%. The scanning speed was always set at 10 μ m/s.

Instrumentation

Refractive index values for the films were determined using the prism coupling method at 632.8, 835, 1310 and 1550 nm (using a Metricon 2010). Using this technique, a measurement accuracy of 0.0005 is obtained and this value was taken as the measurement uncertainty. Refractive index values were measured for both TE and TM modes, but the modes rarely varied by more than the measurement accuracy. Values reported in this paper are averages of the TE and TM results.

Raman Spectroscopy was performed using a Perkin Elmer® Raman Station 400F (785 nm). UV/Vis spectra were recorded using the Perkin Elmer® Lambda 900 UV/Vis/ NIR spectrometer.Electrochemical Impedance Spectroscopy (EIS) was performed using a CHI® Instruments 660A potentiostat. The frequency range scanned ranged from 1 MHz to 1 Hz, and the perturbation signal applied was 100 mV. Platinum and Ag/AgCl were used as the reference and counter electrodes, respectively, and a nF capacitance shunt bridge was used in order to reduce high frequency noise. In house, screen-printed, carbon

paste silver electrodes were used as the working electrode, as described in a previous report [37]. The working electrodes were initially covered in a layer of POT (10-2 M in chloroform) and allowed to dry in order to aid the transfer of ionic to electronic conduction. 40 ⌠Λ of the ionogel to be analysed was then dropcast and photo-polymerised for 10 minutes onto the POT layer. Ionogel thickness was estimated using a Mitutoyo® vernier calipers calibrated to a resolution of 1 μm.

Results and discussion

Spectroscopic characterisation of encapsulated electroactive components

Raman spectroscopy was performed to confirm the encapsulation of the IL and the graphene dispersion within the sol-gel on a molecular level. For comparative purposes, the spectra obtained from the graphene free (material A) and graphene doped material (material C) both containing 40 wt% IL, were superimposed in Fig. 1. The baseline was corrected using the 1800-2000 cm-1 region where no spectral activity was seen, and normalised according to the C-H contributions of both samples at ~2900 cm-1, as both materials should contain the same concentration of organic groups. This approach allows the spectral contributions of the graphene dispersion to be more clearly analysed. The Raman spectroscopy of graphene and its underlying physics are quite well understood and have been the subject of previous reviews [38, 39].

The encapsulation of graphene within the ionogel matrix was confirmed via the presence of the G' band at 2590 cm-1 arising from a two phonon inelastic scattering process; and the disorder induced D' band at 1572 cm-1. An increase in intensity of the band at 1592 cm-1 can be attributed to the doubly degenerate G phonon mode. Spectral contributions from the sol-gel matrix prominent in both spectra include the carbonyl band from MAPTMS present at 1640 cm-1 the C-H polymeric backbone band at 1475 cm-1 plus the confirmation of the

carboxylate bridged zirconium complex at 942 and 976 cm-1, respectively. Equally, the nitrile contribution of the DCA- anion of the IL is seen at 2190 cm-1. These results confirm that the encapsulation of the IL is effective in both materials. In addition, as the intensity and wavenumber of the particular bands of the hybrid sol-gel silicon/zirconium material do not seem to be influenced by the presence of the graphene, which suggests that graphene does not form any covalent bond neither with the sol-gel matrix nor the IL, but is only dispersed within the ionogel.

Electrochemical Impedance Spectroscopy

EIS was performed to estimate the conductivity of the ionogel and the effect of the codoping with graphene particles on a working electrode. For this purpose, in house screen-printed carbon ink electrodes were used.The effect of the hydrolysis degree of the graphene solution on the conductivity has been investigated for materials A, B and C, synthesised with hydrolysis degrees of 10,25 and 50%, respectively, as shown in the Nyquist analyses plotted in Fig. 2. The semicircular arc is indicative of a capacitance effect, the so-called “Warburg tail” and indicates ion diffusion and the x-axis intercept is used to elucidate the resistance to charge transfer of the system analysed. One can observe that the increase of the hydrolysis degree causes a decrease of 81% and 89% compared to material A, in the materials synthesised employing aqueous solutions containing 10 and 25% water to alkoxide groups, respectively. This result can be explained by two phenomena: (1) the

higher concentration of graphene due to the increased hydrolysis degree, owing to its well known favourable conducting properties [40]; and/or (2) the increase of the condensation of the materials as the hydrolysis favours the formation of silanol and hydrous zirconia groups, which inevitably results in the increase of the overall condensation of the material.

In order to clarify the dominant effect on the conductivity of the ionogels, the strategy employed here is to keep the graphene concentration constant, while the concentration of the ZPO precursor is progressively increased to 40 and 50% compared to the organosilane precursor, in materials D and F, respectively. This strategy is based on a previous study by us, which showed that, compared to silicon based alkoxides, transition metal oxides and particularly ZPO exhibits significantly higher reactivity to hydrolysis reactions, leading to more condensed materials [32]. This is mainly due to three structural factors: the increase of sol-gel reactive groups per molecular structure, the increase of the electrophilicity and the decrease of the steric hindrance due to the presence of the organic chain in the MAPTMS precursor.

The Nyquist analyses shown in Fig. 3 depict the relationship between the real and imaginary components of complex impedance for materials A, C, D and F. The results of the Nyquist analyses, as summarised in Table 2, reveal clearly the dependency of the conductivity on the Ionogel formulations, containing the same amount of IL and graphene. By increasing the ZPO complex content, the resultant x-axis intercept is

seen to be inversely decreased, translating to an increase of the overall conductivity. Indeed, taking into account the values in Table 2, a negative slope of 2.376 RCT/mol% of ZPO has been calculated with an R2 > 97%. For the material containing the highest concentration of ZPO (material F), the resistance is decreased by 82%, ultimately resulting in an increase of the conductivity by more than a full order of magnitude through molecular design of the sol-gel matrix. The Bode plot (ii) shows the relationship between the total impedance and the frequency scanned. We observed similar effects for the total impedance as the same condensation trend shifted its value uniformly downward across all frequencies. As all materials were prepared in the same conditions, including the same concentration of IL and graphene, these concentrations should be rigorously identical in all liquid (composed of ionic liquid) and solid phases (composed of the hybrid organic-inorganic sol-gel matrix) of all materials, respectively. However, the increase of the condensation of the materials is well-known to produce a decrease of the porous volume and internal surface area of solid-state materials, the consequence of which should be 1) a better confinement of the IL with a subsequent improved dynamic; and 2) a stronger interaction between the IL and the graphene encapsulated within the solid phase of the ionogel resulting from the proximity effect. In this case, we can believe that both phenomena are probably contributing to the increase of the overall measured conductivity of the developed materials. Nevertheless, the characterisation techniques employed in this study are insufficient to allow precise estimation of the prevalent

phenomenon. We hope to address this critical point in a future study.

Material	Z' (Ω)	R_{CT} decrease (%)	G	σ (S/m)	σ increase (%)
A	12100		8.26 E-05	5.21 E-06	
C	7567	37.46	1.32E-04	8.34 E-06	59.90
D	4185	65.41	2.39 E-04	1.50 E-05	189.12
F	2180	81.98	4.58 E-04	2.89 1E-05	455.04

Table 2: EIS RCT and ionic conductivity estimation.

Optical properties of Ionogels

Optical dispersion and UV-Visible spectroscopy were performed to investigate the homogeneity and the transparency of the resulting gels, as these are critical for the optimisation of the MPP fabrication conditions and their subsequent use as electro- optical devices operating in the visible domain. The optical dispersion curves of materials A and C-E are plotted in Fig.4a. For all wavelengths, the refractive index increases gradually with the increase of ZPO content, resulting in a similar curve evolution. Also, by comparing ionogels A and C, one can observe that the encapsulation of graphene increases the refractive index value by an average value of 1.6x10-3 RIU. This behaviour suggests that the refractive index is directly correlated to the overall molar refraction of the material, and that Ionogels are highly homogeneous. This also supports the conclusion that the densification process and physicochemical modifications tend to occur largely to the

same degree in all ionogels. Furthermore, over the UV-Visible range (Fig.4b), these materials exhibit a strong absorption band located at 325 nm, ascribable to the molecular vibrations of the photoinitiator [41], and also exhibit 100% transparency from 450 to 1000 nm. This suggests that above 450 nm, a multi-photon absorption process is required to induce any radical polymerisation in the UV domain. As our microfabrication setup is tuned at 800nm, the most likely polymerisation process is a second-order process (2PP). Therefore, the possibility to control the refractive index within a large range of values and the high transparency within the visible domain are of particular interest for the fabrication of optical components, where precise control over the optical properties is needed.

3D Laser-fabricated Microstructures

By increasing the concentration of the IL, one can observe the drastic decrease of the mechanical stability of the 3D structures fabricated from material C (Fig. 5). The woodpile fabricated from the IL free material (Fig. 5a) exhibits well-defined straight lines, whereas the material containing 20% IL (Fig. 5b) shows some imperfections in the straightness of the lines. This effect is more pronounced in the materials containing 40 and 50% IL (Fig. 5c and 5d, respectively), where one can clearly observe that some of the lines tend to collapse, demonstrating that the IL dramatically decreases the mechanical resistance and leads to shrinking microstructures. This behaviour can be explained by the significant alterations in the molecular structure, amongst which are the cohesion of the inorganic and organic species (due to the inclusion of both the IL and graphene), the decrease of the photoreactive methacrylate groups per structural unit, as well as the connectivity of the organic network, resulting from the photopolymerisation process. As shown in the TEM image of the IL free material (Fig. 6), the structure can be described as a homogenous dispersion of spherical ZrO2-based nanoparticles (average size 100 nm) within an amorphous organosilane matrix. The negligible shrinkage observed in the IL free material illustrates the high connectivity of the hybrid system, which is due to its characteristic double polymerisation ability. Firstly, the sol-gel synthesis involves the hydrolysis and

polycondensation reactions leading to the formation of strong and irreversible covalent bonds (Si-O-Si and Zr-O-Zr), as previously described [32]. This procedure results in the formation of a soft glass matrix onto which there are covalently attached organic photoreactive methacrylate groups. The MPP process involves the organic radical copolymerisation of the organic groups attached to the inorganic backbone and allows the formation of fully saturated aliphatic C-C covalent bonds that further increase the connectivity of the material. The combination of the sol-gel condensation and the effect of irradiation produce a non-shrinkable material, the structure of which could be described as an inorganic skeleton further rigidified by an organic network. However, the encapsulation of IL within this matrix tends to lessen the connectivity of the sol-gel material and, due to its liquid nature at ambient temperature, the IL further increases the softness of the hybrid system. This is the main reason why the microstructures fabricated from the IL based materials exhibit less rigidity and tend to progressively collapse as a function of increasing IL content. The approach proposed herein consists of balancing the effect of the increased softness arising from the introduction of the IL within the hybrid matrix, through the strengthening of the inorganic network. This can be performed by increasing the zirconate network modifier concentration at the expense of the Ormosil precursor, while keeping the concentration of the IL constant at 50 w/w%.

The microstructures fabricated from materials D and E (40 and 45% ZPO, respectively) both containing 50% IL are shown in Fig. 7. Compared to material C, a clear improvement in the definition and straightness of the lines is observed. A further increase of the inorganic/organic ratio to 50% seems to still produce acceptable structures (Fig. 8a). However, when the inorganic/organic ratio is increased to 60% (material F, Fig. 8b), the mechanical resistance of the woodpile is considerably weakened, as can be seen through the formation of microcracks. Furthermore, it is important to note that the development of the non-irradiated parts of the woodpile were incomplete, demonstrating the dominance of the inorganic character of this material. Generally, the development process is due to the dissolution of the organic moieties of the hybrid system that take away the surrounding inorganic nanoparticles. As the content of the inorganic complex largely exceeds the organic moieties in material G, the structure of the hybrid system is inverted compared to material C. This is confirmed by the TEM image shown in Fig. 9, where the formation of an inorganic network (black zones) is clearly evidenced, in which the organosilicate oligomers are embedded (white zones). In the ionogel, the concentration of the photoreactive groups is further diminished by the high content of IL. Though the absorption at the fabrication wavelength is comparable for all materials (Fig. 4b), the photo- crosslinking process is drastically decreased with the increase of both inorganic complex and IL contents.

Knowing that the desired optimum materials must be a compromise between the conductivity (highest possible content of IL), the photo-processability and the mechanical stability of the fabricated 3D microstructures, as well as high optical quality, materials D, E and F with 50% of IL are the most suitable materials in the series examined in this study.

If ionogel materials are to gain widespread use for many applications, including electrolytes for solar cells, electrochromic displays and sensor devices, ionic liquid confinement and microfabrication techniques of miniaturised devices need to be further developed to prevent IL leaching and to control the spatial definition of the operating systems.

To address these challenges, this study establishes a new route based on photocurable hybrid organic-inorganic sol-gel materials to control the effect of the physico- chemistry of ionogels and accompanying structural limitations, on the mechanical stability of the fabricated microstructures.

It is shown that doping the ionogels with graphene and thereby strengthening the inorganic backbone by the addition of a zirconate network modifier, result in more condensed materials, which increased the conductivity up to a full order of magnitude. The underlying physico-chemical phenomenon has been attributed to the combined effect of a decrease in the porous volume and the internal surface area.

As a result of this, a secondary effect involved an increased confinement of the IL and a strengthened interaction between it and the graphene encapsulated in the solid matrix. Furthermore, the zirconate network modifier has been identified as playing a critical role in the mechanical stability of the three-dimensional microstructures fabricated by multi-photon polymerisation, thus allowing incorporation of higher concentrations of IL within the sol-gel matrices.

The results reported here aim to provide a better understanding of the role of the material formulations and microfabrication requirements in the expanding knowledge of "ionogel *science"*, and contribute to the future development of operating all-solid- states devices with improved functionality.

Acknowledgements

This work is supported by Enterprise Ireland under the grant TD/08/309. CLARITY is supported by Science Foundation Ireland under grant 07/CE/I1147 including the SFI- funded National Access Programme (NAP) grant NAP210 and by Enterprise Ireland grant 07/RFP/MASF812, which is part of EU-MATERA initiative. The authors would like to thank Dr. Fiona Blighe for the preparation of the aqueous graphene dispersions and Dr. Al Robertson of Cytec® industries for the generous donation of the IL used in this study. Authors would also like to thank the LaserLab initiative (ulf-forth001681) and the support provided by the SFI-funded National Access Program (NAP 315).

Figures

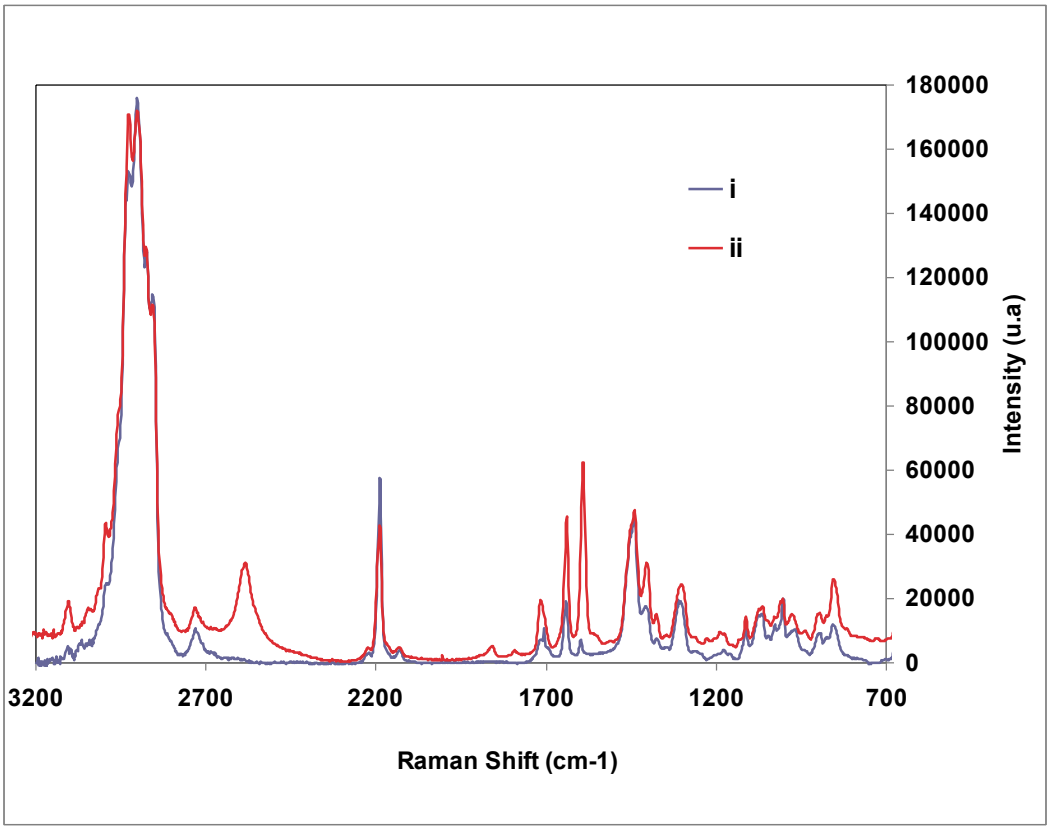

Fig. 1: Raman spectra obtained for materials A (i) and C (ii) both containing 50 wt% [P6,6,6,14][DCA]. Here material A is the parent ionogel without graphene, and material C contains graphene encapsulated within the ionogel.

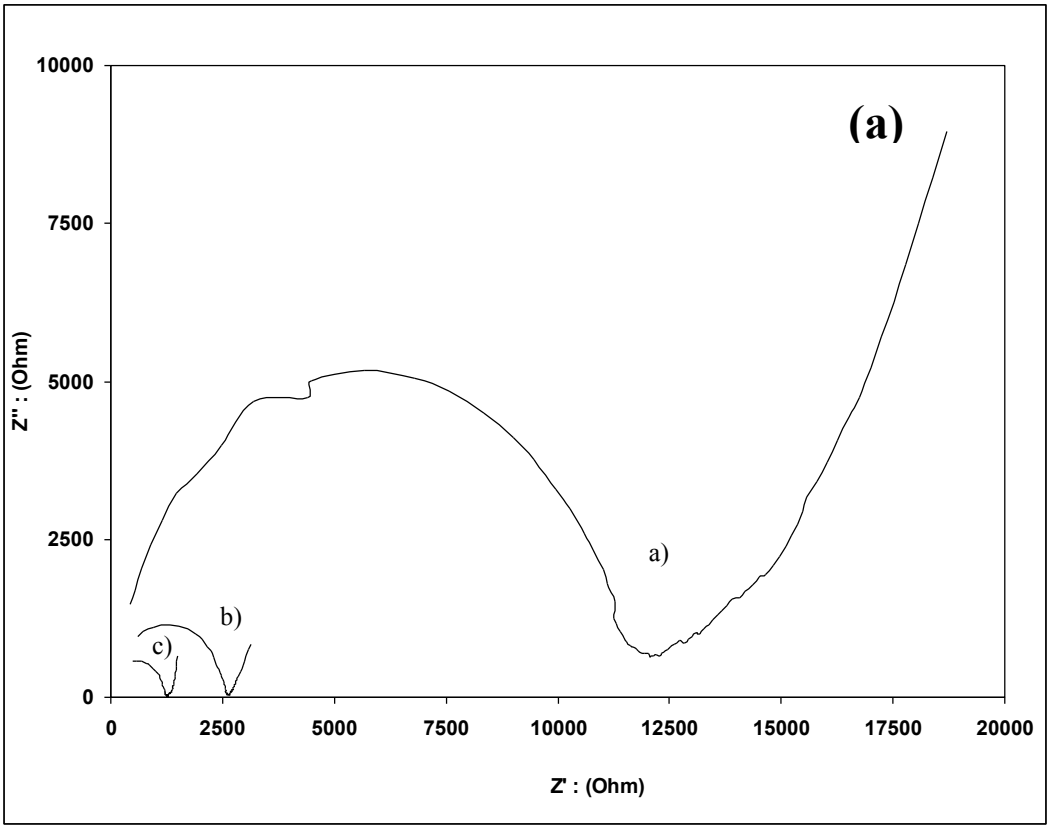
(a)
10000
7500
5000
2500
0
Z'' : (Ohm)
0
2500
5000
7500
10000
12500
15000
17500
20000
Z' : (Ohm)
a)
b)
c)

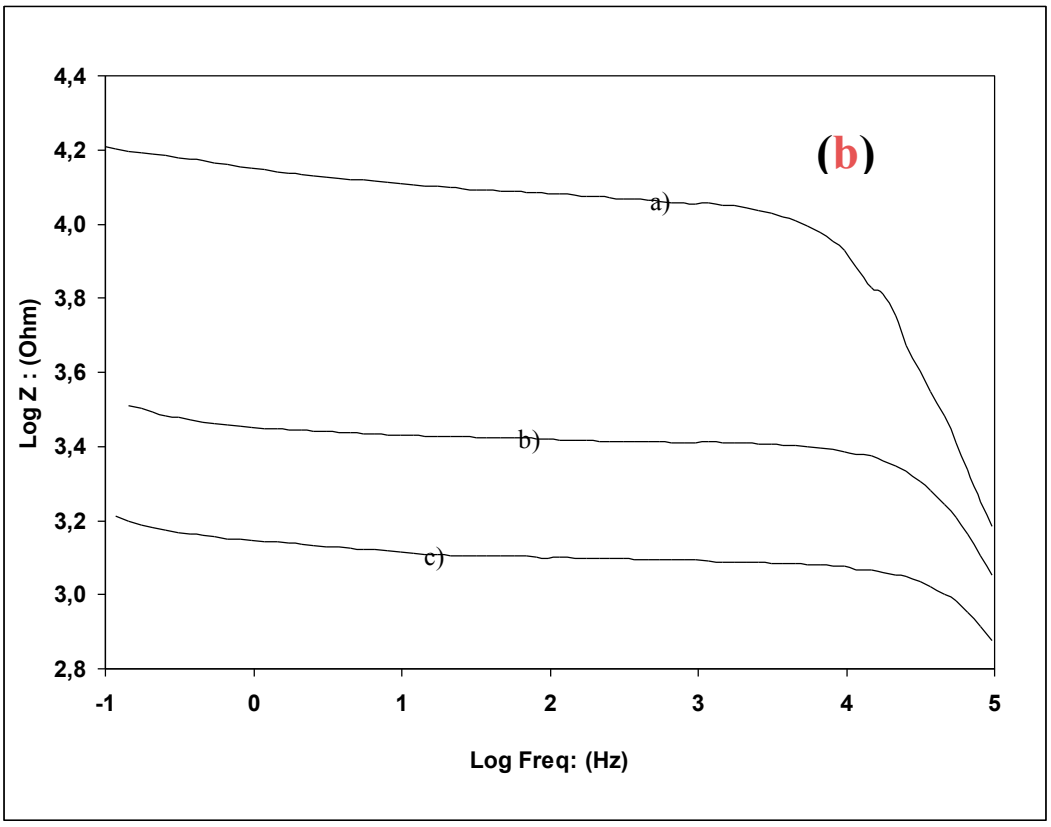
(b)
4,4
4,2
4,0
3,8
3,6
3,4
3,2
3,0
2,8
Log Z : (Ohm)
-1
0
1
2
3
4
5
Log Freq: (Hz)
a)
b)
c)

Fig. 2: (a) Nyquist plot analysis and **(b)** Bode plot analysis of for materials A (a), B (b) and C (c) containing 40% IL.

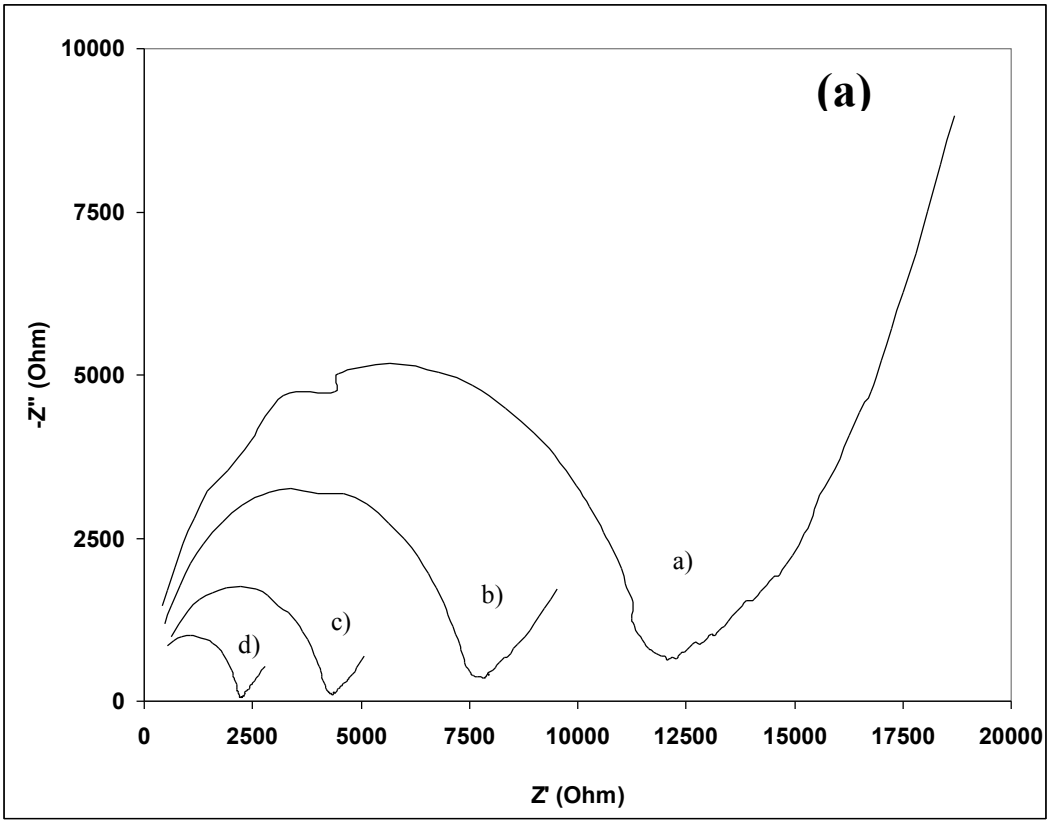
(a)
10000
7500
5000
2500
0
-Z'' (Ohm)
0
2500
5000
7500
10000
12500
15000
17500
20000
Z' (Ohm)
a)
b)
c)
d)

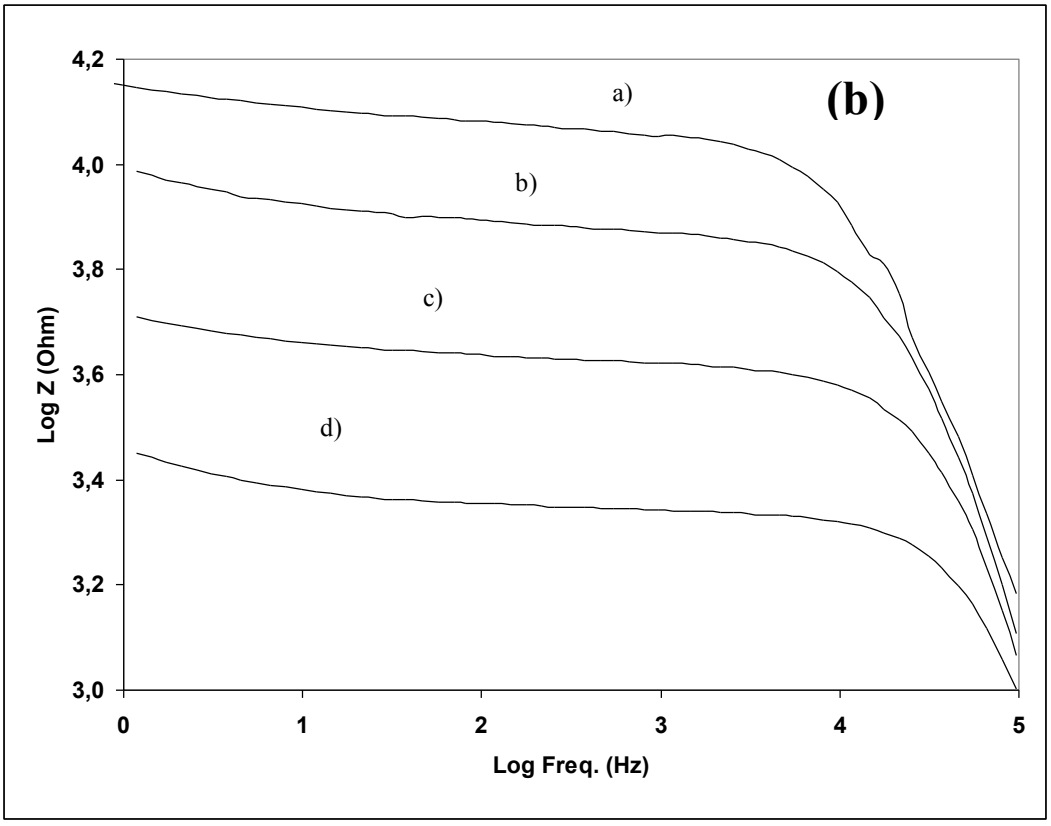
(b)
4,2
4,0
3,8
3,6
3,4
3,2
3,0
Log Z (Ohm)
0
1
2
3
4
5
Log Freq. (Hz)
a)
b)
c)
d)

Fig. 3: (a) Nyquist plot analysis and (b) Bode plot analysis of graphene encapsulated ionogels composed of 40% of IL in (a) material A, (b) material D, (c) material E and material F.

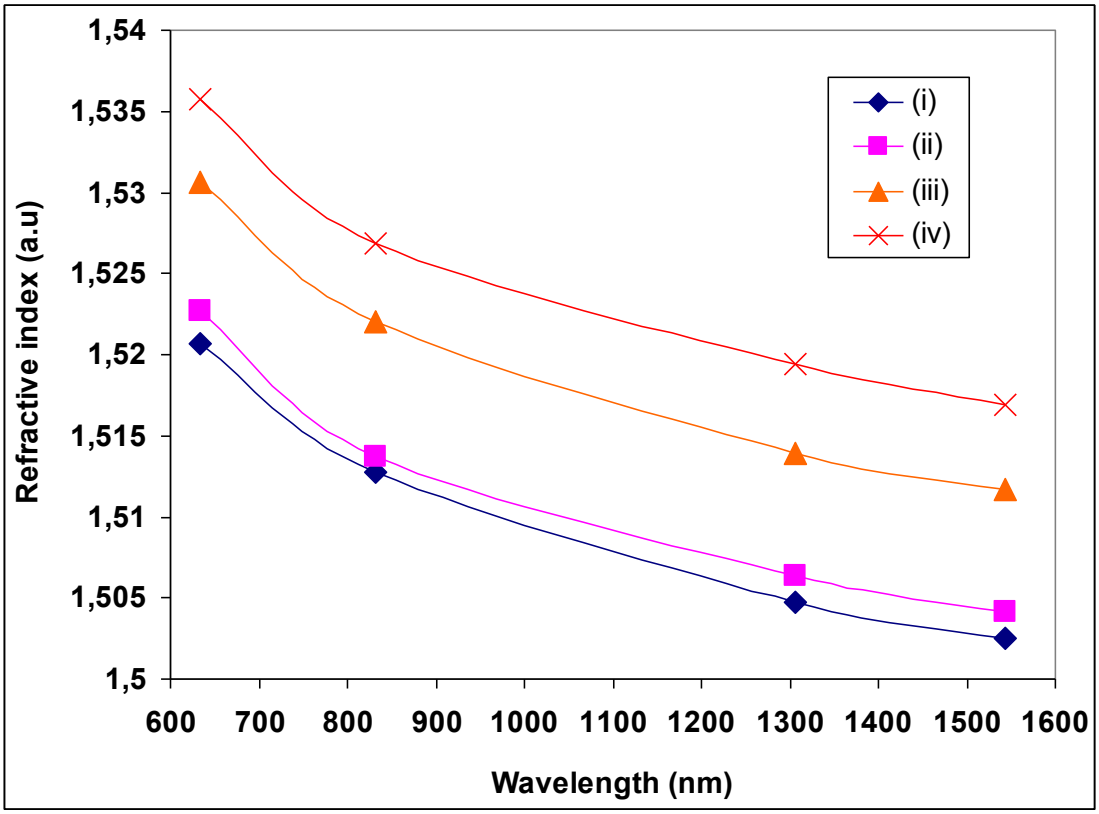

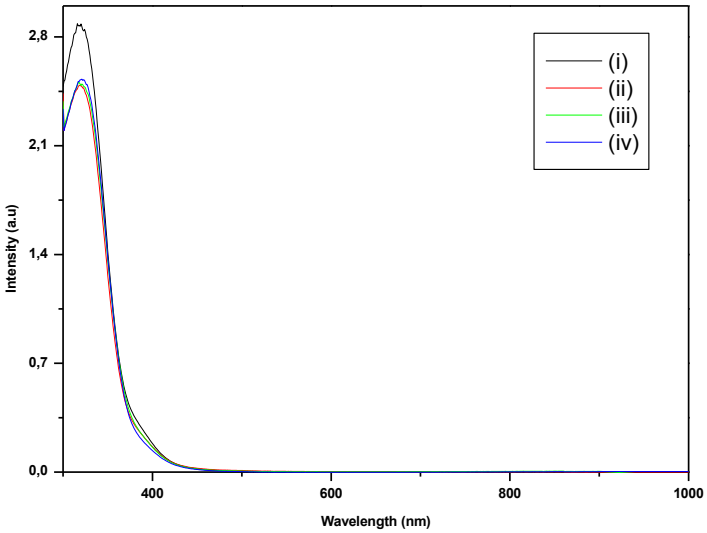

Fig. 4. Optical dispersion curves (a) and UV-Vis aborption spectra (b) of materials A (i), C (ii), D (iii) and E (iv) all containing 50 wt% [P6,6,6,14][DCA].

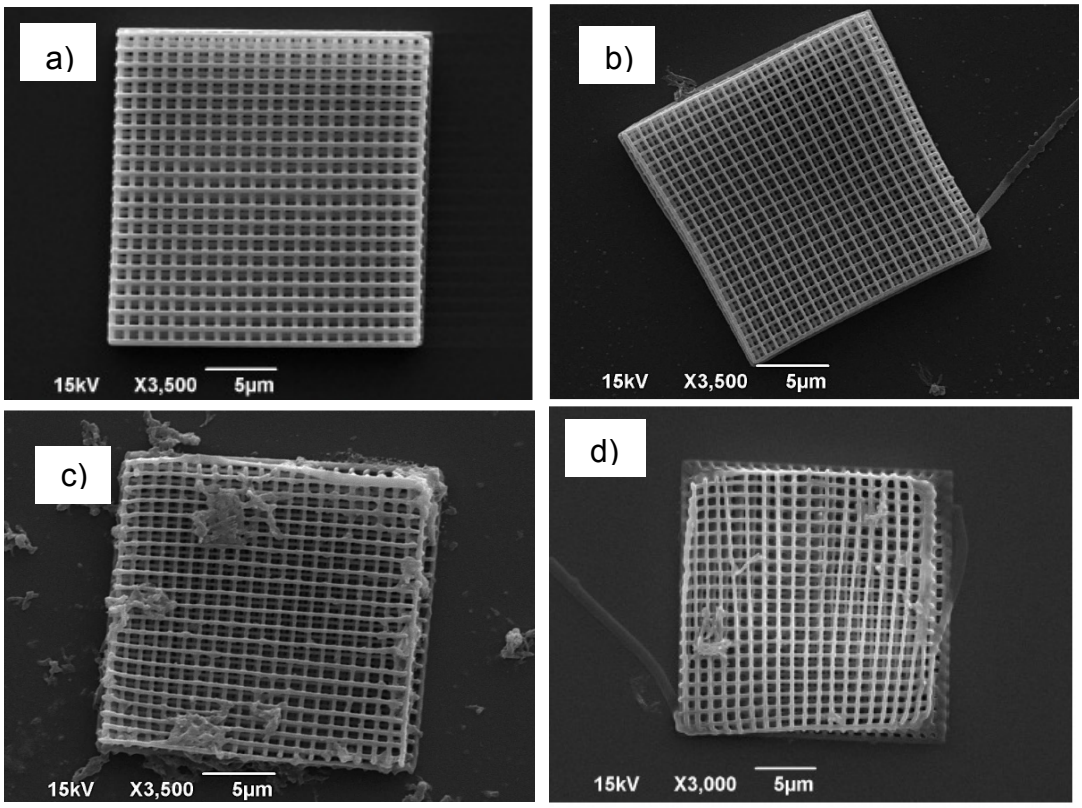

Fig. 5: SEM images of woodpiles fabricated from material C containing different amount of IL a) 0%, b) 20%, c) 40% and d) 50%.

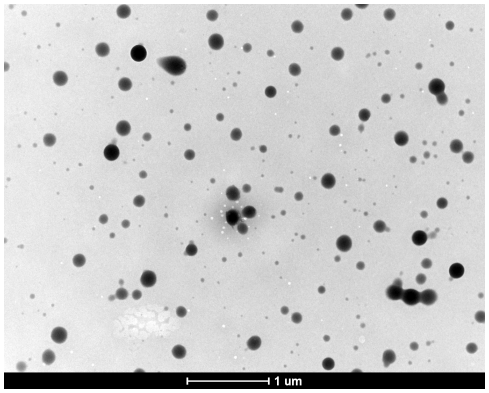

Fig. 6: TEM image of material C.

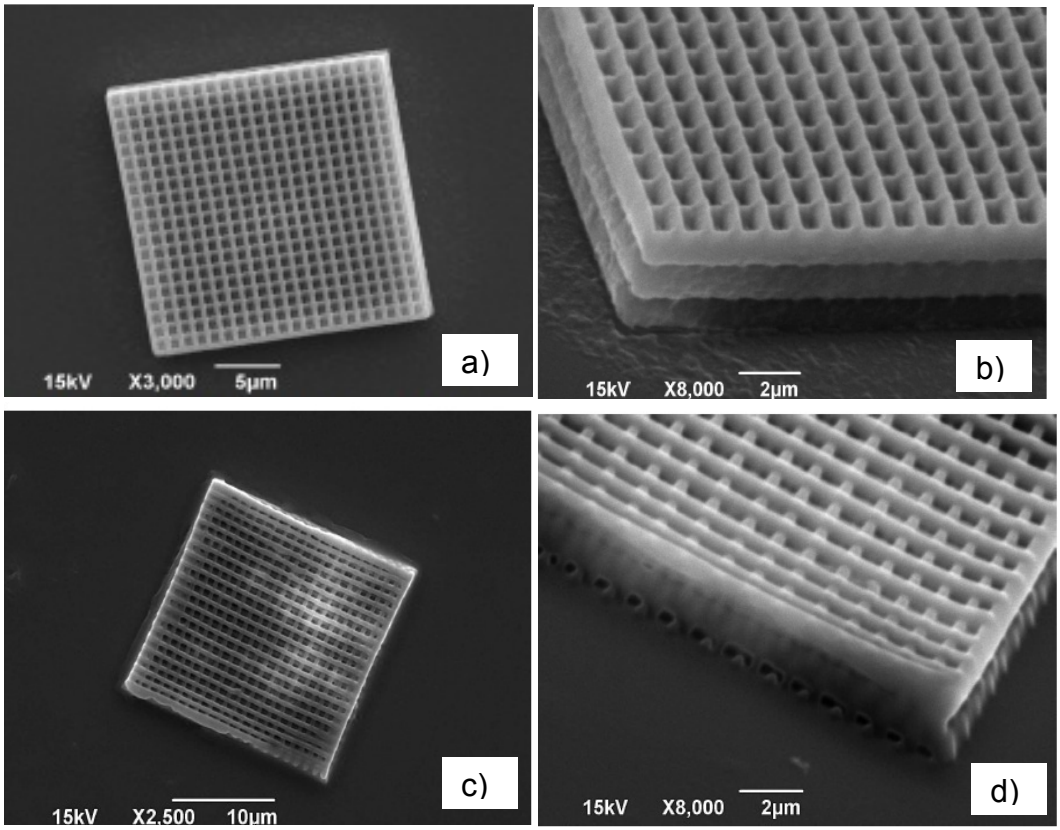

Fig. 7: SEM images of woodpiles fabricated from materials D (a, b) and E (c, d), both containing 50% of IL.

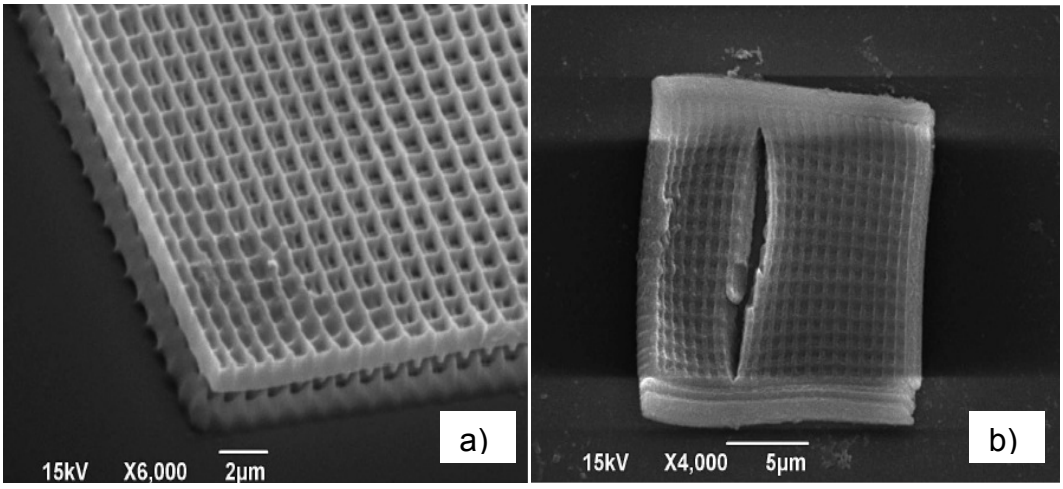

Fig. 8: SEM images of woodpiles fabricated from materials F (a) and G (b), both containing 50% of IL.

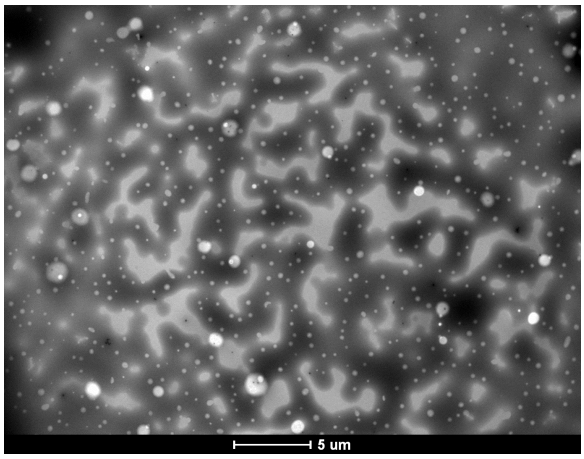

Fig. 9: TEM image of material G.

References

[1] J. C. Ribot, C. Guerrero-Sanchez, R. Hoogenboom and U. S. Schubert, *J. Mater. Chem.,* 2010, **20,** 8279.

[2] A. Vioux, L. Viau, S. Volland and J. Le Bideau, *C. R. Chim.,* 2010, **13,** 242.

[3] Jean Le Bideau, Lydie Viau and André Vioux, *Chem. Soc. Rev.,* 2011, **40,** 907.

[4] S. T. Handy, *Curr. Org. Chem.,* 2005, **9,** 959.

[5] H. Weingaertner, *Angew. Chem. Int. Ed.,* 2008, **47,** 654.

[6] Ze Yu, Nick Vlachopoulos, Mikhail Gorlov and Lars Kloo, *Dalton Trans.,* 2011, **40,** 10289.

[7] Nathalie Cheminet, Thibaut Jarrosson, Jean-Pierre Lère-Porte, Françoise Serein-Spirau, Luiz Cury, Joel Moreau, Lydie Viau and André Vioux, *J. Mater. Chem.,* 2011, **21,** 13588.

[8] Srivastava Sachin K.; Gupta Banshi D. *Sens. Actuators, B,* 2011, **156,** 559.

[9] C. Schmidt, T. Gluck and G. Schmidt-Naake, *Chem. Eng. Technol.,* 2008, **31,** 13.

[10] T. Ueki and M. Watanabe, *Macromolecules,* 2008, **41,** 3739.

[11] M. Antonietti, D. B. Kuang, B. Smarsly and Z. Yong, *Angew. Chem. Int. Ed.,* 2004, **43,** 4988.

[12] M.L. Zheludkevich, I.Miranda Salvado,M.G.S. Ferreira, *J. Mater. Chem.,* 2005, **15,** 5099.

[13] M. Guglielmi, *J. Sol–Gel Sci. Technol.,* 1997, **8,** 443.

[14] C. Sanchez, B. Julian, P. Belleville, M. Popall, *J. Mater. Chem.,* 2005, **15,** 3559.

[15] C.J. Brinker, G. Scherrer, Sol–Gel Science: The Physics and Chemistry of Sol–Gel Processing, Academic Press, San Diego, CA, 1990.

[16] C. Sanchez, P. Gomez-Romero, Functional Hybrid Materials, Wiley VCH,Wein-heim, 2004, ISBN- 13-978-3-527-30484-4.

[17] Ronald Gobel, Peter Hesemann, Jens Weber, Eleonore Moller, Alwin Friedrich, Sabine Beuermanna and Andreas Taubert, *Phys. Chem. Chem. Phys.,* 2009, **11,** 3653.

[18] J. Le Bideau, P. Gaveau, S. Bellayer, M.-A. Neouze and A. Vioux, *Phys. Chem. Chem. Phys.,* 2007, **9,** 5419.

[19] Jones Brad H., Lodge Timothy P., *Chem. Mater.,* 2011, **23,** 4824.

[20] K. T. Lee, J. C. Lytle, N. S. Ergang, S. M. Oh and A. Stein, *Adv. Funct. Mater.,* 2005, **15,** 547.

[21] F. Tuinstra and J. L. Koenig, *J. Chem. Phys.,* 1970, **53,** 1126.

[22] Yongchao Si and Edward T. Samulski, *Nano Lett.,* 2008, **8,** 1679.

[23] Sacha Stankovich, Dmitriy A. Dikin, Richard D. Piner, Kevin A. Kohlhaas, Alfred Kleinhammes, Yuanyuan Jia, Yue Wu, SonBinh T. Nguyen, Rodney S. Ruoff, *Carbon,* 2007, **45,** 1558.

[24] Gyeong Sook Bang, Hye-Mi So, Mi Jin Lee and Chi Won Ahn, *J. Mater. Chem.,* 2012, **22,** 4806.

[25] Zhuang-Jun Fan, Wang Kai, Jun Yan, Tong Wei, Lin-Jie Zhi, Jing Feng, Yue-ming Ren, Li-Ping Song and Fei Wei, *ACS Nano,* 2011, **5,** 191.

[26] E. Lahiff, C. Lynam, N. Gilmartin, R. O'Kennedy and D. Diamond, *Anal. Bioanal. Chem.,* 2010, **398,** 1575.

[27] J. B. Ducros, N. Buchtova, A. Magrez, O. Chauvet and J. Le Bideau, *J. Mater. Chem.,* 2011, **21,** 2508.

[28] T. Fukushima, *Polym. J.,* 2006, **38,** 743.

[29] I. Ahmad, U. Khan and Y. K. Gun'ko, *J. Mater. Chem.,* 2011, **21,** 16990.

[30] J. Lee and T. Aida, *Chemical Communications,* 2011, **47,** 6757.

[31] Andrew Kavanagh, Robert Copperwhite, Mohamed Oubaha, Jessica Owens, Colette McDonagh, Dermot Diamonda and Robert Byrne, *J. Mater. Chem.,* 2011, **21,** 8687.

[32] M. Oubaha, M. Smaihi, P. Etienne, P. Coudray, Y. Moreau, *J. Non-Cryst. Solids,* 2003, **318,** 305.

[33] M. J. Earle, J. Esperanca, M. A. Gilea, J. N. C. Lopes, L. P. N. Rebelo, J. W. Magee, K. R. Seddon and J. A. Widegren, *Nature,* 2006, **439,** 831.

[34] V. Melissinaki, A. A. Gill, I. Ortega, M. Vamvakaki, A. Ranella, J. W. Haycock, C. Fotakis, M. Farsari, and F. Claeyssens, *Biofabrication,* 2011, **3,** 045005.

[35] I. Sakellari, A. Gaidukeviciute, A. Giakoumaki, D. Gray, C. Fotakis, M. Farsari, M. Vamvakaki, C. Reinhardt, A. Ovsianikov, and B. N. Chichkov, *Appl. Phys. A,* 2010, **100,** 359.

[36] M. Farsari, M. Vamvakaki, B.N. Chichkov, *J. Opt.,* 2010, **12,** 124001.

[37] A. Morrin, A. J. Killard and M. R. Smyth, *Anal. Lett.,* 2003, **36,** 2021.

[38] Ferrari, A. C., *Solid State Commun.,* 2007, **143,** 47.

[39] Malard, L. M.; Pimenta, M. A.; Dresselhaus, G.; Dresselhaus, M. S., *Phys. Rep.,* 2009, **473,** 51.

[40] U. Khan, I. O'Connor, Y. K. Gun'ko, J. N. Coleman, *Carbon,* 2010, **48,** 2825.

[41] M. Oubaha, R. Copperwhite, C. Boothman, A. Ovsianikov, R. Kiyan, V. Purlys, M. O'Sullivan, C. McDonagh, B. Chichkov, R. Gadonas, B. D. MacCraith. *J. Mater. Sci.,* 2011, **46,** 400.